



Fourier Transform Light Scattering (FTLS) of Cells and Tissues

Huafeng Ding¹, Zhuo Wang¹, Freddy Nguyen², Stephen A. Boppart², Larry J. Millet³,
Martha U. Gillette³, Jianming Liu⁴, Marni Boppart⁴, and Gabriel Popescu^{1,*}

¹Quantitative Light Imaging Laboratory, Department of Electrical and Computer Engineering,
Beckman Institute for Advanced Science and Technology,

²Biophotonics Imaging Laboratory, Department of Electrical and Computer Engineering,
Beckman Institute for Advanced Science and Technology,

³Department of Cell and Developmental Biology,

⁴Department of Kinesiology and Community Health, Beckman Institute for Advanced Science and Technology,
University of Illinois at Urbana-Champaign, Urbana, IL 61801, USA

Fourier transform light scattering (FTLS) has been recently developed as a novel, ultrasensitive method for studying light scattering from inhomogeneous and dynamic structures. FTLS relies on quantifying the optical phase and amplitude associated with a coherent image field and propagating it numerically to the scattering plane. In this paper, we review the principle and applications of FTLS to static and dynamic light scattering from biological tissues and live cells. Compared with other existing light scattering techniques, FTLS has significant benefits of high sensitivity, speed, and angular resolution. We anticipate that FTLS will set the basis for disease diagnosis based on intrinsic tissue optical properties and provide an efficient tool for quantifying cell structures and dynamics.

Keywords: Fourier Transform Light Scattering, Quantitative Phase Microscopy, Scattering, Phase, Tissue, Cells.

CONTENTS

1. Introduction	1
2. Principle of FTLS	4
3. Phase Retrieval	5
4. FTLS of Microsphere (System Calibration)	5
5. FTLS of Tissues	6
6. FTLS of Cells	8
7. FTLS On Red Blood Cell (RBC) Dynamics	10
8. Summary and Outlook	10
References	11

1. INTRODUCTION

Elastic (static) light scattering (ELS) has emerged as an important approach in the field for studying biological samples, as it is noninvasive, requires minimum sample preparation, and extracts rich information about morphology and dynamic activity.^{1–9} In ELS, by measuring the angular distribution of the scattered field, one can infer quantitative information about the sample structure (i.e.,

its spatial distribution of refractive index). Light scattering by cells and tissues evolved as a dynamic area of study, especially because this type of investigation can potentially offer a non-invasive window into function and pathology.^{10–13} Despite all these efforts, light scattering-based studies currently have limited use in the clinic. A great challenge is posed by the insufficient knowledge of the tissue optical properties. Dynamic light scattering (DLS) has been intensively applied to investigate inhomogeneous and dynamic systems, including live cells.^{14–17} More recently, the mechanical properties of a complex fluid have been examined by detecting dynamic scattering from the probing particles.^{18,19} Thus, the viscoelastic properties of complex fluids are retrieved over various temporal scales. This method was further extended to the cell membranes with attached micron-sized beads as probes, which provides a new way to study the microrheology of live cells.²⁰

Light scattering techniques provide information that is intrinsically averaged over the measurement volume. Thus, the spatial resolution is compromised and the scattering contributions from individual component are averaged.

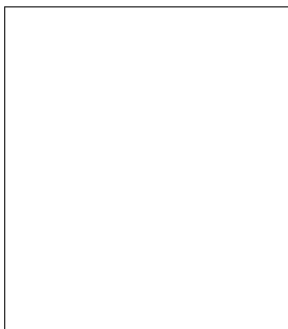
*Author to whom correspondence should be addressed.



Huafeng Ding received the B.Sc. degree in applied physics from Nankai University, Tianjin, China, in 2000 and his Ph.D. degree in biomedical physics from East Carolina University, Greenville, NC USA, in 2006. He is currently a postdoctoral research associate with Beckman Institute for Advanced Science and Technology, Department of Electrical and Computer Engineering, University of Illinois at Urbana-Champaign, IL USA. His research interest is in development of new optical techniques to study biological tissues and cells and also in application of those novel tools to early diagnosis of disease or treatment planning. He is now working on the application of the Fourier Transform Light Scattering to study the structure and dynamic activity of biological tissues and live cells.



Zhuo Wang received his B.S. degree (with honors) in precision instruments, measurement and control from Tsinghua University, Beijing, in 2002, and the M.S. degree in Electrical Engineering from Wayne State University in 2006. He worked two and half years as an optical engineer at Tsinghua-Foxconn nanotechnology research center after he got his B.S. degree. He is currently a research assistant in the Department of Electrical and Computer Engineering at University of Illinois at Urbana-Champaign. His research interests include biosensors, quantitative light imaging, biooptics and nanotechnology.



Freddy Nguyen is an M.D.-Ph.D. Candidate in the Department of Chemistry, University of Illinois at Urbana-Champaign. He is affiliated with the Beckman Institute for Advanced Science and Technology, the College of Medicine, and the Medical Scholars Program. He is currently holds a pre-doctoral fellowship from the Department of Defense's Congressionally Directed Medical Research Programs—Breast Cancer Program. Prior to being at the University of Illinois, he was at the G.R. Harrison Spectroscopy Laboratory at M.I.T. as a research engineer. Mr. Nguyen received his B.S. degree in Chemistry and B.A. in Mathematics from Rice University in Houston, TX. His research interests have broadly been in the development of spectroscopic and imaging techniques and their associated contrast agents for direct biomedical applications such as cancer and atherosclerosis.



Stephen A. Boppart is Professor of Electrical and Computer Engineering, Bioengineering, and Medicine, and is Head of the Biophotonics Imaging Laboratory at the Beckman Institute for Advanced Science and Technology on the campus of the University of Illinois at Urbana-Champaign. He is currently leading a campus-wide Imaging Initiative to build a community of research faculty and staff around the science, technology, and application of imaging. Boppart received his B.S. and M.S. degrees in electrical engineering from the University of Illinois at Urbana-Champaign in 1990 and 1991, respectively. After conducting government laser safety research from 1991 to 1993, he returned to graduate studies, completing his Ph.D. in medical and electrical engineering from MIT in 1998, and his M.D. in medicine from Harvard Medical School in 2000. He completed his internship and residency training in internal medicine at the University of Illinois. His research interests include the development

of novel optical imaging technologies for biological and medical applications, with particular emphasis on translating these to clinical applications in cancer detection and diagnosis. Professor Boppart is a Fellow of the Optical Society of America and International Society for Optical Engineering, ~~the International Society for Optical Engineering~~, and a Member of the Society for Molecular Imaging, the Academy of Molecular Imaging, the American Association for the Advancement of Science, the American Association for Cancer Research, and the American Medical Association. He was named one of the Top 100 Innovators in the World by the Technology Review Magazine for his research in medical technology in 2002. He received the IEEE Engineering in Medicine and Biology Society Early Career Achievement Award in 2005, and in 2009, was recognized with the Paul F. Forman Engineering Excellence Award from the Optical Society of America for his dedication and advancement in undergraduate research education.



Larry J. Millet is a postdoctoral research associate in Micro and Nanotechnology and manager of the BioNanotechnology Lab in the College of Engineering at the University of Illinois Urbana-Champaign. In 2009 he received his Ph.D. in Cell and Developmental Biology while working with Martha Gillette. His work focused on controlling the microenvironment local to neurons for achieving low-density neuronal analysis *in vitro*. Prior to attending the University of Illinois at Urbana-Champaign, he received his BS. in Biology from Portland State University and worked in the research and technology development division within Intel Corporation. His research focuses on resolving mechanisms that regulate cell structure and function by crossing levels of analysis through a multidisciplinary approach. Dr. Millet is a member of the Society for Neuroscience and the Biomedical Engineering Society.



Martha U. Gillette is professor of Cell and Developmental Biology, Physiology and Neuroscience, and is affiliated with Bioengineering, the Beckman Institute, Institute for Genomic Biology and the Micro and NanoTechnology Labs. Gillette received her B.A. from Grinnell College, Ph.D. in developmental biology from the University of Toronto, and postdoctoral training in neuroscience at the University of California, Santa Cruz. Her research at multiple levels seeks to understand the actions of molecules in nerve cells, signal processing in brain, and their consequences for what animals do. She is engaged in cross-disciplinary research bridging campus excellence in cellular neuroscience, nano-scale analytical chemistry and materials engineering. Her discoveries have important health applications: malfunctioning of the master circadian timing system results in brain and organ dysfunction, which manifest as clinical disorders of sleep, affect and neural degeneration. She has been a Beckman Scholar, Center for Advanced Study

Fellow, University Scholar and in 2005 became Cell and Developmental Biology Alumni Professor of the University of Illinois. She has mentored nearly 50 graduate and post-doctoral trainees, the majority of whom are women, and received the Outstanding Advisor Award for medical scholar training. She has served in numerous advisory capacities to the NIH, and in executive positions in professional.



Jianming Liu received his B.A. from Nankai University, Tianjin, China, in 2002 and his Ph.D. in Cell and developmental Biology from University of Illinois at Urbana-Champaign in 2007. He was a postdoctoral research associate with Beckman Institute for Advanced Science and Technology, Department of Kinesiology and Community Health, University of Illinois at Urbana-Champaign. His research interest is to study stem cells pluripotency and cell fate specification using myogenic pathway as a model. He is also interested in signaling pathways that are important for muscle development, physiology and pathogenesis of muscle diseases. He is currently a postdoctoral fellow at University of California San Francisco and supported by American heart association postdoctoral fellowship.



Marni Boppert is an Assistant Professor in the College of Applied Health Sciences, University of Illinois at Urbana-Champaign (UIUC), and holds a full-time faculty appointment at the Beckman Institute. She received her B.S. in Cell Biology from the University of New Hampshire, M.S. in Cell Biology from Creighton University, Sc.D. in Applied Anatomy and Physiology from Boston University, and postdoctoral training in Cell and Developmental Biology from UIUC. Her current research interests include cellular biomechanics, cell signaling, and the synergistic role of stem cells and extracellular matrix in the protection of skeletal muscle from injury, disease, and aging.



Gabriel Popescu is an Assistant Professor in the Department of Electrical and Computer Engineering, University of Illinois at Urbana-Champaign and holds a full faculty appointment with the Beckman Institute for Advance Science and Technology. He is also an affiliate faculty in the Bioengineering Department. Professor Popescu received the B.S. and M.S. in Physics from University of Bucharest, in 1995 and 1996, respectively. He obtained his M.S. in Optics in 1999 and the Ph.D. in Optics in 2002 from the School of Optics/CREOL (now the College of Optics and Photonics), University of Central Florida. Dr. Popescu continued his training with the G.R. Harrison Spectroscopy Laboratory at M.I.T., working as a postdoctoral associate. He joined UIUC in August 2007. His current research combines microscopy, holography, interferometry and scattering techniques to study cell structure and dynamics at the nanoscale.

Particle tracking microrheology has been recently proposed to measure the particle displacements in the imaging (rather than scattering) plane,^{21,22} in which the spatial resolution is reserved. However, the drawback is that relatively large particles are needed such that they can be tracked individually, which also limits the throughput required for significant statistical average. Recently, *phase-sensitive* methods have been employed to directly extract the refractive index of cells and tissues.^{23,24} From this information, the angular scattering can be achieved via the Born approximation.²⁵

To overcome some of these limitations, we developed FTLS as an approach to study light scattering from biological samples based on diffraction phase microscopy (DPM).²⁶ FTLS combines the high spatial resolution associated with optical microscopy and intrinsic averaging of light scattering techniques.²⁷ Due to its common path interferometric geometry, DPM is stable in optical path-length to the sub-nanometer level. This feature allows FTLS perform studies on static and dynamic samples with unprecedented sensitivity.

2. PRINCIPLE OF FTLS

Our FTLS system requires accurate phase retrieval for elastic light scattering (ELS) measurements and, in

addition, fast acquisition speed for DLS studies.^{13,27} Figure 1 depicts our experimental setup that satisfies these requirements by incorporating a common path interferometer with a commercial computer-controlled microscope. The second harmonic of a Nd:YAG laser ($\lambda = 532$ nm) is used to illuminate the sample in transmission. To ensure full spatial coherence, the laser beam is coupled into a single mode fiber and further collimated by a fiber collimator. The light scattered by the sample is collected by the objective lens of the microscope (AxioObserver Z1, Zeiss) and imaged at the side port of the microscope. A diffraction grating G is placed at this image plane, thus generating multiple diffraction orders containing full spatial information about the image. In order to establish a common-path Mach-Zehnder interferometer, a standard spatial filtering lens system L_1 – L_2 is used to select the two diffraction orders and generate the final interferogram at the CCD plane. The 0th order beam is low-pass filtered using the spatial filter SF positioned in the Fourier plane of L_1 , such that at the CCD plane it approaches a uniform field. Simultaneously, the spatial filter allows passing the entire frequency content of the 1st diffraction order beam and blocks all the other orders. The 1st order is thus the imaging field and the 0th order plays the role of the reference field. The two beams propagate along a common optical path, thus significantly reducing the longitudinal phase

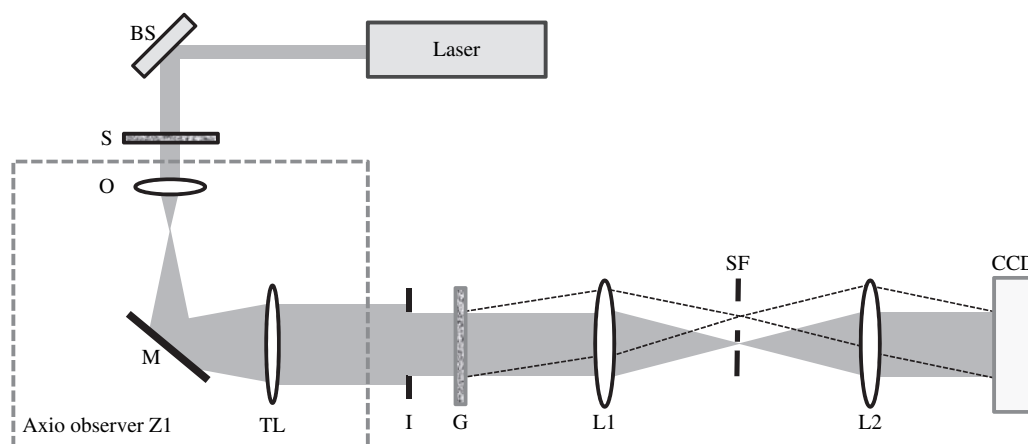


Fig. 1. FTLS experimental setup. BS, beam splitter; S, sample; O, objective lens; M, mirror; TL, tube lens; I, iris; G, Grating; SF, spatial filter; L1 and L2, lenses. Adapted with permission from Ref. [13], H. F. Ding et al., *Opt. Lett.* 34, 1372 (2009). © 2009.

noise. The direction of the spatial modulation is along the x -axis, such that the total field at the CCD plane has the form.²⁶

$$U(x, y) = |U_0|e^{i(\phi_0+\beta x)} + |U_1(x, y)|e^{i\phi_1(x, y)} \quad (1)$$

In Eq. (1), $|U_{0,1}|$ and $\phi_{0,1}$ are the amplitudes and the phases of the orders of diffraction 0, 1, while β represents the spatial frequency shift induced by the grating to the 0th order. To preserve the transverse resolution of the microscope, the spatial frequency β exceeds the maximum frequency allowed by the numerical aperture of the instrument. The L_1 - L_2 lens system has an additional magnification of $f_2/f_1 = 5$, such that the sinusoidal modulation of the image is sampled by 4 CCD pixels per period. The obtained interferograms were used to calculate the phase information of the objects as followed.

3. PHASE RETRIEVAL

The complex analytic signal formalism of time-varying fields has been of interest for many applications in optics since its introduction by Gabor.²⁸ Specifically, a real function $u(t)$ and its Hilbert transform $\tilde{u}(t)$ represent the real and the imaginary parts of a complex analytic signal. This Hilbert transformation has been commonly used to retrieve phase shifts from single temporal interferograms and for fringe pattern analysis.²⁸ In our phase measurement, a single spatial interferogram recorded by the CCD is processed for the retrieval of a full-field phase image. For a given sample the spatially varying irradiance at the image plane across either the x or the y axis has the form²⁸

$$I(x) = I_R + I_s(x) + 2[I_R I_s(x)]^{1/2} \cos[qx + \phi(x)] \quad (2)$$

where I_R is the reference irradiance distribution and I_s is the sample irradiance distributions, q is the spatial frequency of the fringes, and ϕ is the spatially varying phase associated with the object. For the transparent objects of interest here (i.e., live cells), $I_s(x)$ is expected to be nearly homogeneous, i.e., to have a weak dependence on x or y . We performed Fourier transform on the varying irradiance in Eq. (2)

$$\tilde{I}(\mathbf{q}) \propto \iint I(x, y) e^{i[q_x x + q_y y]} dx dy \quad (3)$$

and then applied a spatial high-pass filter to isolate the cross term,

$$u(x) = 2[I_R I_s(x)]^{1/2} \cos[qx + \phi(x)] \quad (4)$$

The corresponding imaginary part of complex analytic signal associated with the real function $u(x)$ can be obtained through a Hilbert Transform,

$$\tilde{u}(x) = i \frac{P}{2} \int_{-\infty}^{\infty} \frac{u(x')}{x - x'} dx' \quad (5)$$

In Eq. (5) the right-hand side stands for a principal-value integral and is the Hilbert transform of $u(x)$.^{26, 28, 29} Therefore the phase associated with the analytic signal is calculated as²⁸

$$\Phi(x) = \tan^{-1} \left(\frac{\tilde{u}(x)}{u(x)} \right) \quad (6)$$

where Φ is strongly wrapped since the analytic signal exhibits rapid phase modulation with frequency q . However, as we mentioned early in the section 2, q is higher than the spatial-frequency content of the object, the unwrapping procedure works efficiently. Finally, the phase associated with the object is extracted as $\phi(x) = \Phi(x) - qx$.²⁸ Thus, from a single CCD exposure, we obtain the spatially-resolved phase and amplitude associated with the image field.

From this image field information \tilde{U} , the complex field can be numerically propagated at arbitrary planes; in particular, the far-field angular scattering distribution \tilde{U} can be obtained simply via a Fourier transformation,²⁷

$$\tilde{U}(\mathbf{q}, t) = \int U(\mathbf{r}, t) e^{-i\mathbf{q}\cdot\mathbf{r}} d^2\mathbf{r} \quad (7)$$

With time lapse image acquisition, the temporal scattering signals are recorded and the sampling frequency is only limited by the speed of the camera. The power spectrum is obtained through Fourier transform of this time resolved scattering signals.

4. FTLS OF MICROSPHERE (SYSTEM CALIBRATION)

As the system calibration, we applied FTLS to dilute microsphere water suspensions sandwiched between two cover slips, the scattering of which can be easily modeled with Mie calculation.²⁷ The measured complex field associated with such samples can be expressed as²⁷

$$U(\mathbf{r}; t) = \iint_A U_F(\mathbf{r}') \sum_{i=1}^N \delta\{\mathbf{r} - \mathbf{r}_i(t) - \mathbf{r}'\} d^2\mathbf{r}' \quad (8)$$

In Eq. (8), U_F is the (time-invariant) complex field associated with each particle, δ is the 2D Dirac function describing the position (x_i, y_i) of each of the N moving particles, and the integral is performed over the microscope field of view A .

Figures 2(a–b) shows the amplitude and phase distributions obtained by imaging 3 micron polystyrene beads at a particular point in time. For ELS studies, prior to processing the interferogram, we subtract a background image obtained as the intensity map without sample or reference beam. The scattered far-field is obtained by Fourier transforming Eq. (8) in space. This angular field distribution factorizes into a *form* field \tilde{U}_F , which is determined by the angular scattering of a single particle, and a *structure* field \tilde{U}_S , describing the spatial correlations in particle positions,²⁷

$$\tilde{U}(\mathbf{q}; t) = \tilde{U}_F(\mathbf{q}) \tilde{U}_S(\mathbf{q}; t) \quad (9)$$

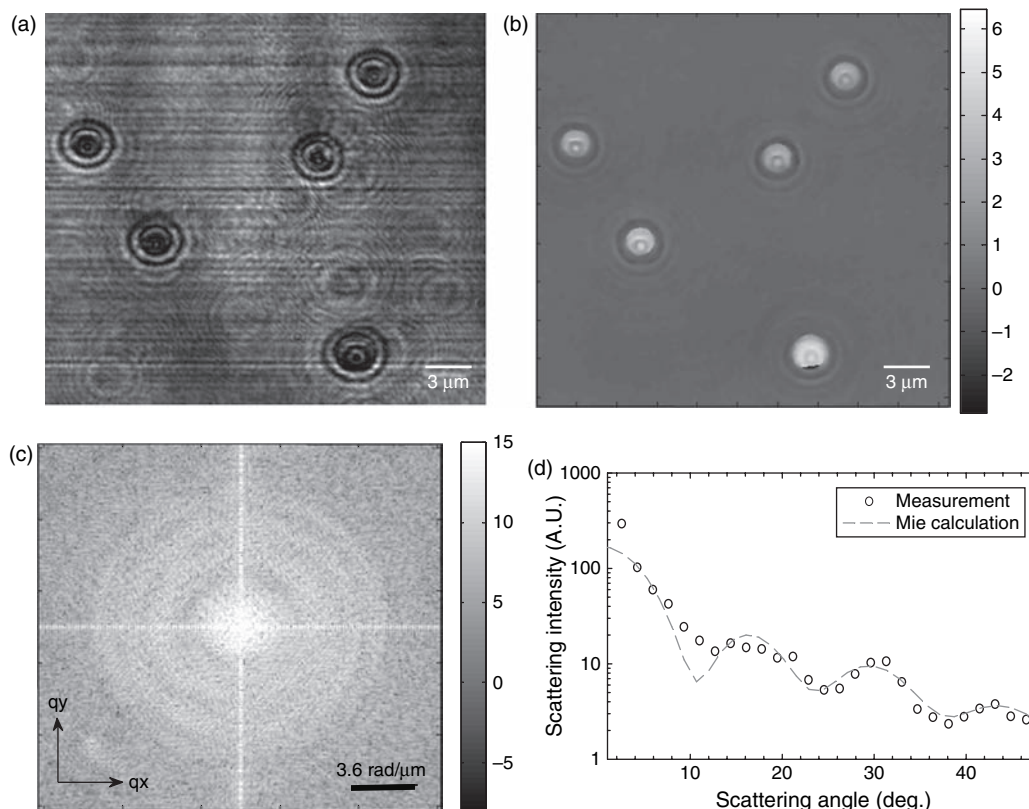


Fig. 2. FTLS reconstruction procedure of angular scattering from $3\ \mu\text{m}$ beads. (a) Amplitude image. (b) Reconstructed phase image. (c) Scattering wave vector map. (d) Retrieved angular scattering and comparison with Mie calculation. Adapted with permission from Ref. [27], H. F. Ding et al., *Phys. Rev. Lett.* 101, 238101 (2008). © 2008.

where \mathbf{q} is the spatial wave vector and $\tilde{U}_S(\mathbf{q}; t) = \sum_i e^{i\mathbf{q}\cdot\mathbf{r}_i(t)}$. Figure 2(c) shows the resulting intensity distribution $|\tilde{U}_F(\mathbf{q})|^2$ for the beads in 2(a–b). As expected for such sparse distributions of particles, the form function is dominant over the entire angular range. However, by finding the phase-weighted centroid of each particle, FTLS can retrieve independently the structure function whenever it has a significant contribution to the far-field scattering, e.g., in colloidal crystals. The scattered intensity (e.g., Fig. 2(c)) is averaged over rings of constant wave vectors, $q = (4\pi/\lambda) \sin(\theta/2)$, with θ the scattering angle, as exemplified in Figure 2(d). In order to test the ability of FTLS to retrieve quantitatively the form function of the spherical dielectric particles, we used Mie theory for comparison.³⁰ The oscillations in the angular scattering establish the quantitative agreement between the FTLS measurement and Mie theory, which contrasts with the common measurements on colloidal suspensions, where the signal is averaged over a large number of scatterers.

5. FTLS OF TISSUES

Upon propagation through inhomogeneous media such as tissues, optical fields suffer modifications in terms of irradiance, phase, spectrum, direction, polarization, and coherence, which can reveal information about the sample of

interest. We use FTLS to extract quantitatively the scattering mean free path l_s and anisotropy factor g from tissue slices of different organs.¹³ This direct measurement of tissue scattering parameters allows predicting the wave transport phenomena within the organ of interest at a multitude of scales. The scattering mean free path l_s was measured by quantifying the attenuation due to scattering for each slice via the Lambert-Beer law, $l_s = -d/\ln[I(d)/I_0]$, where d is the thickness of the tissue, $I(d)$ is the irradiance of the unscattered light after transmission through the tissue, and I_0 is the total irradiance, i.e., the sum of the scattered and unscattered components. The unscattered intensity $I(d)$, i.e., the spatial DC component, is evaluated by integrating the angular scattering over the diffraction spot around the origin. The resulting l_s values for 20 samples for each organ, from the same rat are summarized in Figure 3(a).

The anisotropy factor g is defined as the average cosine of the scattering angle,

$$g = \frac{\int_{-1}^1 \cos(\theta) p[\cos(\theta)] d[\cos(\theta)]}{\int_{-1}^1 p[\cos(\theta)] d[\cos(\theta)]} \quad (10)$$

where p is the normalized angular scattering, i.e., the phase function. Note that, since Eq. (7) applies to tissue

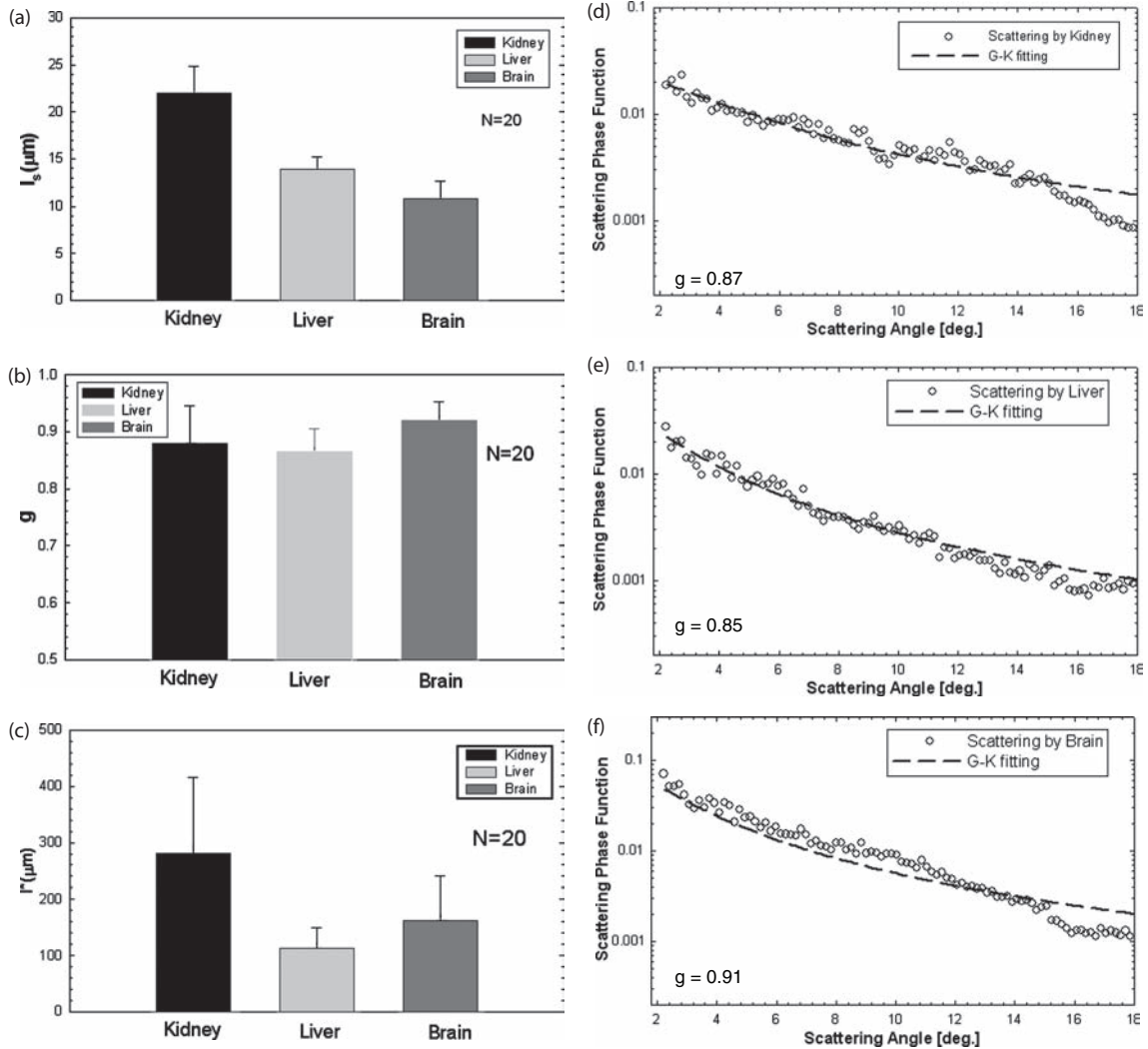


Fig. 3. FTLS measurements of the scattering mean free path l_s (a), anisotropy factors (b) and transport mean free path (c) for the three rat organs with 20 samples per group. The error bars correspond to the standard deviations ($N = 20$). (d–f) The angular scattering plots associated with the scattering maps in Figures 2(d–f). The dash lines indicate fits with the G–K phase function. Adapted with permission from Ref. [13], H. F. Ding et al., *Opt. Lett.* 34, 1372 (2009). ©2009.

slices of thickness $d < l_s$, it cannot be used directly in Eq. (10) to extract g since g values in this case will be thickness-dependent. This is so because the calculation in Eq. (10) is defined over tissue of thickness $d = l_s$, which describes the average scattering properties of the tissue (i.e., independent of how the tissue is cut). Under the weakly scattering regime of interest here, this angular scattering distribution p is obtained by propagating the complex field numerically through $N = l_s/d$ layers of $d = 5$ microns thickness,¹³

$$p(\mathbf{q}) \propto \left| \iint [U(\mathbf{r})]^N e^{i\mathbf{q}\cdot\mathbf{r}} d^2\mathbf{r} \right|^2 \quad (11)$$

Equation (11) applies to a slice of thickness l_s . It reflects that, by propagating through N weakly scattering layers of tissue, the total phase accumulation is the sum of the phase shifts from each layer, as is typically assumed in phase

imaging of transparent structures.³¹ The angular scattering distribution, or phase function, $p(\theta)$ is obtained by performing azimuthal averaging of the scattering map, $p(\mathbf{q})$, associated with each tissue sample. The maximum scattering angle was determined by the numeric aperture of the objective lens and it is about 18° for our current setup ($10\times$ objective applied for tissue study). The angular scattering data were further fitted with Gegenbauer Kernel (GK) phase function³²

$$P(\theta) = ag \cdot \frac{(1-g^2)^{2\alpha}}{\pi [1+g^2-2g\cos(\theta)]^{(\alpha+1)} [(1+g)^{2\alpha} - (1-g)^{2\alpha}]} \quad (12)$$

Note that g can be estimated directly from the angular scattering data via its definition (Eq. (10)). However, because of the limited angular range measured, g tends to be overestimated by this method, and, thus, the GK fit offers a

more reliable alternative than the widely used Henyey-Greenstein (HG) phase function with the parameter $a = 1/2$. The representative fitting plots for each sample are shown in Figures 3(d–f). The final values of g are included in Figure 3(b) and agree very well with previous reports in the literature.³³ From these measurements of thin, singly scattering slices, we inferred the behavior of light transport in thick, strongly scattering tissue. Thus the transport mean free path, which is the renormalized scattering length to account for the anisotropic phase function, can be obtained as $l^* = l_s/(1 - g)$. The l^* values for 20 samples from each organ are shown in Figure 3(c).

In order to extend the FTLS measurement towards extremely low scattering angles, we scanned large fields of view by tiling numerous high-resolution microscope images.²⁷ Figure 4(a) presents a quantitative phase map of a 5 micron thick tissue slice obtained from the breast of a rat model by tiling $\sim 1,000$ independent images. This 0.3 giga-pixel composite image is rendered by scanning the sample with a 20 nm precision computerized translation stage. The phase function associated with this sample is shown in Figure 4(b). We believe that such a broad angular range, of almost 3 decades, is measured here for the first time and cannot be achieved via any single measurement. Notably, the behavior of the angular scattering follows power laws with different exponents, as indicated by the two dashed lines. This type of measurements over

broad spatial scales may bring new light into unanswered questions, such as tissue architectural organization and possible self similar behavior.³⁴

The results above showed that FTLS can quantify the angular scattering properties of thin tissues, which thus provides the scattering mean free path l_s and anisotropy factor g for the macroscopic (bulk) organ. We note that, based on the knowledge of l_s , g , and l^* , one can predict the outcome of a broad range of scattering experiments on large samples (size $\gg l^*$), via numerical solutions to the transport equation, or analytical solutions to the diffusion equation. We envision that the FTLS measurements of unstained tissue biopsies, which are broadly available, will provide not only diagnosis value, but possibly the premise for a large scattering database, where various tissue types, healthy and diseased, will be fully characterized in terms of their scattering properties.

6. FTLS OF CELLS

Light scattering investigations can noninvasively reveal subtle details about the structural organization of cells.^{7, 8, 35–38} We employed FTLS to measure scattering phase functions of different cell types and demonstrate its capability as a new modality for cell characterization.³⁹ In order to demonstrate the potential of FTLS for cell sorting based on the rich scattering signals that it provides, we retrieved the scattering phase functions from three cell groups (Figs. 5(a–c)): red blood cells, myoblasts (C2C12), and neurons. Figures 5(d–f) show the angular scattering distributions associated with these samples. For each group, we performed measurements on different fields of view. Remarkably, FTLS provides these scattering signals over approximately 35 degrees ($40\times$ objective applied for cell study) in scattering angle and several decades in intensity. For comparison, we also measured the scattering signature of the background (i.e., culture medium with no cells in the field of view by using threshold), which incorporates noise contributions from the beam inhomogeneities, impurities on optics, and residues in the culture medium. These measurements demonstrate that FTLS is sensitive to the scattering signals from single cells, which contrast to previous measurements on cells in suspensions. Subtle details of the cell structures may be washed in studies on suspensions since the signals are averaged over various cell orientations.

We analyzed our FTLS data with a statistical algorithm based on the principle component analysis (PCA) aimed at maximizing the differences among the cell groups and providing an automatic means for cell sorting.⁴⁰ This statistical method mathematically transforms the data to a new coordinate system to illustrate the maximum variance by multiplying the data with the chosen individual vectors. Our procedure can be summarized as follows. First, we average the n ($n = 1 \dots 45$) measurements for the 3 cell

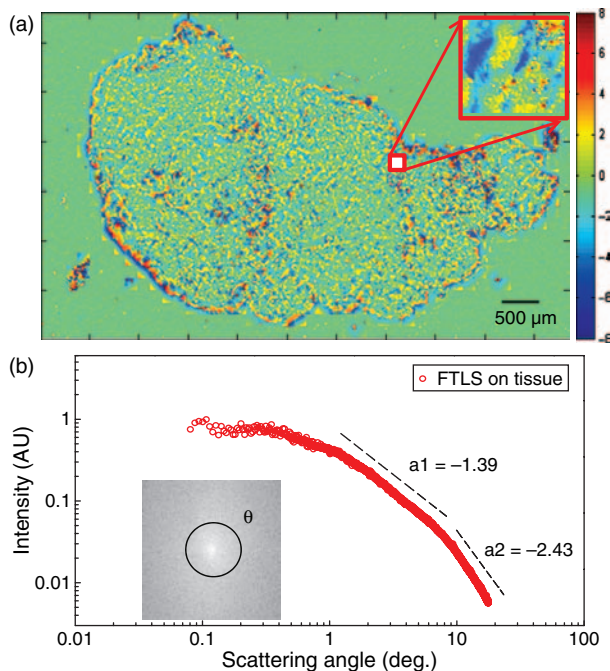


Fig. 4. (a) Terra-pixel quantitative phase image of a mouse breast tissue slice. Color bar indicates phase shift in radians. (b) Angular scattering from the tissue in (c). The inset shows the 2D scattering map, where the average over each ring corresponds to a point in the angular scattering curve. The dashed lines indicate power laws of different exponents. Adapted with permission from Ref. [27], H. F. Ding et al., *Phys. Rev. Lett.* 101, 238101 (2008). © 2008.

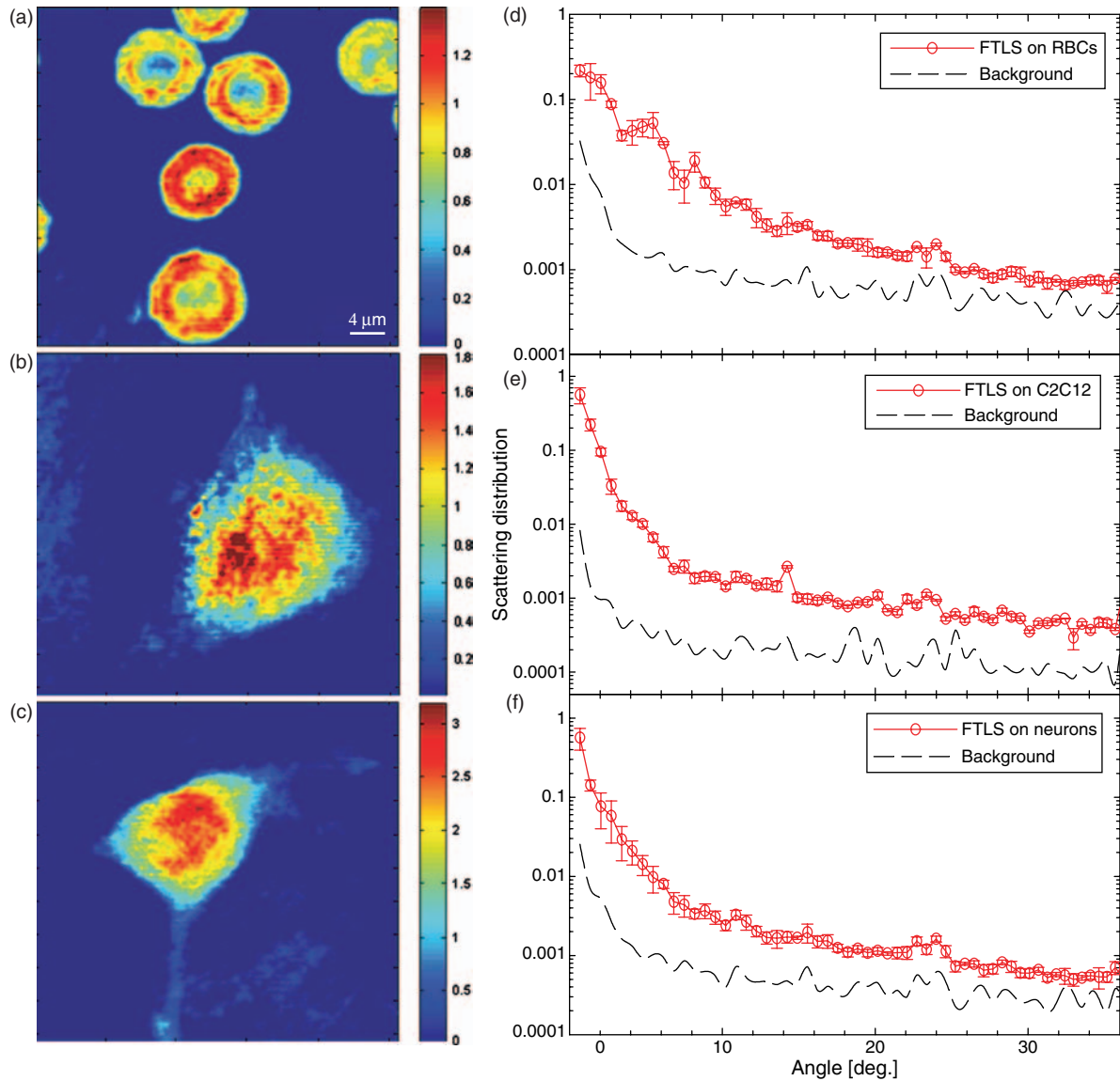


Fig. 5. (a–c) Quantitative phase images of red blood cells (a), C2C12 cell (b), and neuron (c); the scale bar is 4 microns and the color bar indicates phase shift in radians. (d–e) Respective scattering phase functions measured by FTLS. Adapted with permission from [39], H. Ding et al., *Opt. Lett.*, submitted.

types (15 measurements per group), to obtain the average scattered intensity, $\overline{I}(\theta_m) = 1/45 \sum_{n=1...45} I_n(\theta_m)$, with $m = 1 \dots 35$ denoting the number of scattering angles. Second, we generate a matrix ΔY_{nm} of variances, where n indexes the different measurements and m the scattering angles. The covariance matrix associated with ΔY , $\text{Cov}(\Delta Y)$, is calculated and its eigenvalues and eigenvectors extracted. The three principal components are obtained by retaining three eigenvectors corresponding to the largest eigenvalues. In order to build the training set, 45 measurements (i.e., 15 per cell type) were taken and processed following the procedures described above.

Figure 6 shows a representation of the data where each point in the plot is associated with a particular FTLS measurement. In addition to the 15 measurements per group

for the training sets, we performed, respectively, 15, 15, and 10 test measurements for neurons, RBCs, and C2C12 cells. The additional test measurements allowed us to evaluate the sensitivity and specificity of assigning a given cell to the correct group.⁴¹ We obtained sensitivity values of 100%, 100% and 70%, and specificities of 100%, 88% and 100% for RBCs, neurons and C2C12 cells, respectively.

We demonstrated here that FTLS can be used to differentiate between various cell types. Due to the particular imaging geometry used, scattering phase functions associated with single cells can be retrieved over a broad range of angles. This remarkable sensitivity to weak scattering signals may set the basis for a new generation of cytometry technology, which, in addition to the intensity information, will extract the structural details encoded in the phase

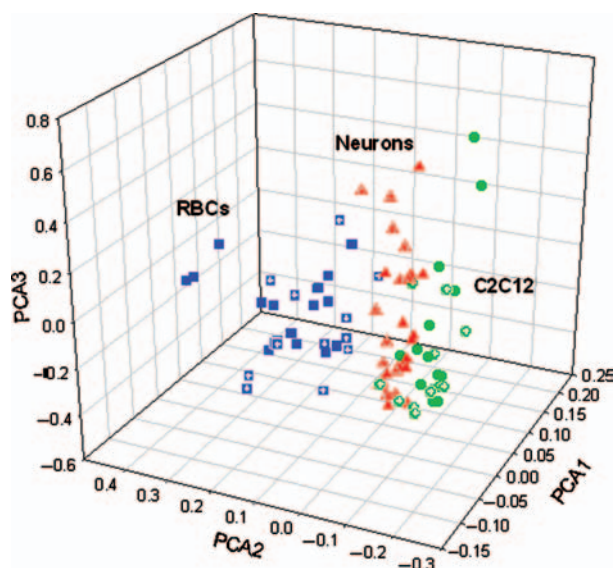


Fig. 6. PCA of the experimental data for the three cell types, as indicated. Solid filled symbols are the training sets of these three different biological samples included inside three ellipses. The symbols with “+” sign in the middle are the testing measurements for each sample.

of the optical field. FTLS may improve on fluorescence-based flow cytometry as it operates without the need for exogenous tags.

7. FTLS ON RED BLOOD CELL (RBC) DYNAMICS

Dynamic properties of cell membrane components such as actin and microtubulus have been the subject of intense scientific interest.^{42–46} In particular, it has been shown that actin filaments play an important role in various aspects of cell dynamics, including cell motility.^{43,44} In this section, we briefly discussed the application of FTLS to study the fluctuating membranes of RBCs.²⁷ To determine how the cell membrane flickering contributes to the dynamic light scattering of cells, RBCs from healthy volunteer sandwiched with two glass cover slips were imaged via DPM by acquiring 256 frames, at 20 frames per s, about 14 s. Figure 7(a) shows the membrane displacement histograms of a RBC. The power spectrum in Figure 7(b) follows power laws with different exponents in time for all scattering angles (or, equivalently, wave vectors). As expected, the slower frequency decay at larger q -values indicates a more solid behavior, i.e., the cell is more compliant at longer spatial wavelengths. Notably, the exponent of -1.36 of the longer wavelength (5 degree angle), is compatible with the -1.33 value predicted by Brochard et al. for the fluctuations at each point on the cell.⁴⁷ This is expected, as at each point the motions are dominated by long wavelengths.⁴⁸ The dynamic FTLS studies of RBC rheology can be performed on many cells simultaneously, which is an advantage over the previous flickering studies.^{29,47,49}

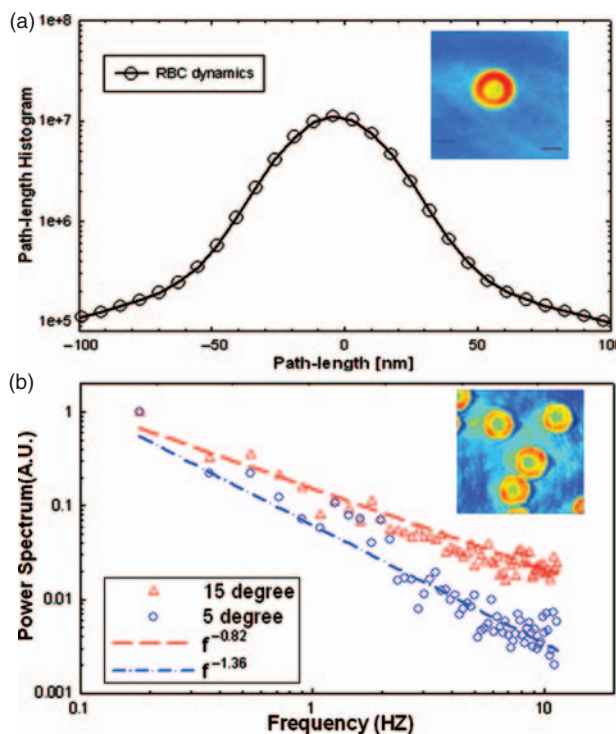


Fig. 7. (a) Histogram of the path-length displacements of a red blood cell. The inset is the phase image. (b) Dynamics FTLS of red blood cells: log-log power spectra at 5 and 15 degrees with the respective power law fits, as indicated. The inset shows one RBC phase image from the time sequence. Adapted with permission from Ref. [27], H. F. Ding et al., *Phys. Rev. Lett.* 101, 238101 (2008). © 2008.

We believe that these initial results are extremely promising and that the label-free approach proposed here for studying cell dynamics will complement very well the existing fluorescence studies. Currently, we are working to extend the dynamics light scattering study to more complex cells and extract information from the temporal light scattering signals associated with the activity of individual cell component such as filamentous actin and microtubules. The polymerization and depolymerization of these components are highly dynamic processes and have important functional roles.⁵⁰

8. SUMMARY AND OUTLOOK

In summary, we discussed the high sensitivity dynamic light scattering study with FTLS. Due to the interferometric experimental geometry and the reliable phase retrieval, spatial resolution of the scatterer positions is well preserved. FTLS has been applied to study the tissue optical properties, cell type characterization and dynamic structure of cell membrane. We anticipate that this type of measurement will enable new advances in life sciences for its ability to detect weak scattering signals over broad temporal (milliseconds to hours) and spatial (fraction of microns to centimeters) scales. Current efforts in our laboratory are

focused on advancing the technique to study the mechanic properties of cells including the cell membrane tension, bending modulus and 3D shear modulus.

References

1. R. Drezek, A. Dunn, and R. Richards-Kortum, *Appl. Opt.* 38, 3651 (1999).
2. J. R. Mourant, M. Canpolat, C. Brocker, O. Esponda-Ramos, T. M. Johnson, A. Matanock, K. Stetter, and J. P. Freyer, *J. Biomed. Opt.* 5, 131 (2000).
3. C. S. Mulvey, A. L. Curtis, S. K. Singh, and I. J. Bigio, *IEEE J. Sel. Top. Quant.* 13, 1663 (2007).
4. H. Ding, J. Q. Lu, R. S. Brock, T. J. McConnell, J. F. Ojeda, K. M. Jacobs, and X. H. Hu, *Journal of Biomedical Optics* 12, 034032 (2007).
5. M. T. Valentine, A. K. Popp, D. A. Weitz, and P. D. Kaplan, *Opt. Lett.* 26, 890 (2001).
6. W. J. Cottrell, J. D. Wilson, and T. H. Foster, *Opt. Lett.* 32, 2348 (2007).
7. A. Wax, C. H. Yang, V. Backman, K. Badizadegan, C. W. Boone, R. R. Dasari, and M. S. Feld, *Biophys. J.* 82, 2256 (2002).
8. V. Backman, M. B. Wallace, L. T. Perelman, J. T. Arendt, R. Gurjar, M. G. Muller, Q. Zhang, G. Zonios, E. Kline, T. McGillican, S. Shapshay, T. Valdez, K. Badizadegan, J. M. Crawford, M. Fitzmaurice, S. Kabani, H. S. Levin, M. Seiler, R. R. Dasari, I. Itzkan, J. Van Dam, and M. S. Feld, *Nature* 406, 35 (2000).
9. F. Charriere, N. Pavillon, T. Colomb, C. Depeursinge, T. J. Heger, E. A. D. Mitchell, P. Marquet, and B. Rappaz, *Opt. Express* 14, 7005 (2006).
10. V. V. Tuchin, *Tissue Optics*, SPIE - The International Society for Optical Engineering (2000).
11. J. W. Pyhtila, K. J. Chalut, J. D. Boyer, J. Keener, T. D'Amico, M. Gottfried, F. Gress, and A. Wax, *Gastrointest Endosc* 65, 487 (2007).
12. L. Q. H. Fang, E. Vitkin, M. M. Zaman, C. Andersson, S. Salahuddin, L. M. Kimerer, P. B. Cipolloni, M. D. Modell, B. S. Turner, S. E. Keates, I. Bigio, I. Itzkan, S. D. Freedman, R. Bansil, E. B. Hanlon, and L. T. Perelman, *Appl. Opt.* 46, 1760 (2007).
13. H. F. Ding, F. Nguyen, S. A. Boppart, and G. Popescu, *Opt. Lett.* 34, 1372 (2009).
14. B. J. Berne and R. Pecora, *Dynamic Light Scattering with Applications to Chemistry, Biology and Physics*, Wiley, New York (1976).
15. D. J. Pine, D. A. Weitz, P. M. Chaikin, and E. Herbolzheimer, *Phys. Rev. Lett.* 60, 1134 (1988).
16. M. Suissa, C. Place, E. Goillot, B. Berge, and E. Freyssingeas, *Epl-Europhys. Lett.* 78 (2007).
17. D. Watson, N. Hagen, J. Diver, P. Marchand, and M. Chachisvilis, *Biophys. J.* 87, 1298 (2004).
18. T. G. Mason and D. A. Weitz, *Phys. Rev. Lett.* 74, 1250 (1995).
19. F. Gittes, B. Schnurr, P. D. Olmsted, F. C. MacKintosh, and C. F. Schmidt, *Phys. Rev. Lett.* 79, 3286 (1997).
20. M. S. Amin, Y. Park, N. Lue, R. R. Dasari, K. Badizadegan, M. S. Feld, and G. Popescu, *Opt. Express* 15, 17001 (2007).

21. T. G. Mason, K. Ganesan, J. H. vanZanten, D. Wirtz, and S. C. Kuo, *Phys. Rev. Lett.* 79, 3282 (1997).
22. J. C. Crocker, M. T. Valentine, E. R. Weeks, T. Gisler, P. D. Kaplan, A. G. Yodh, and D. A. Weitz, *Phys. Rev. Lett.* 85, 888 (2000).
23. N. Lue, J. Bewersdorf, M. D. Lessard, K. Badizadegan, K. Dasari, M. S. Feld, and G. Popescu, *Opt. Lett.* 32, 3522 (2007).
24. B. Rappaz, P. Marquet, E. Cuhe, Y. Emery, C. Depeursinge, and P. J. Magistretti, *Opt. Express* 13, 9361 (2005).
25. W. Choi, C. C. Yu, C. Fang-Yen, K. Badizadegan, R. R. Dasari, and M. S. Feld, *Opt. Lett.* 33, 1596 (2008).
26. G. Popescu, T. Ikeda, R. R. Dasari, and M. S. Feld, *Opt. Lett.* 31, 775 (2006).
27. H. F. Ding, Z. Wang, F. Nguyen, S. A. Boppart, and G. Popescu, *Phys. Rev. Lett.* 101, 238104 (2008).
28. T. Ikeda, G. Popescu, R. R. Dasari, and M. S. Feld, *Opt. Lett.* 30, 1165 (2005).
29. G. Popescu, T. Ikeda, K. Goda, C. A. Best-Popescu, M. Laposata, S. Manley, R. R. Dasari, K. Badizadegan, and M. S. Feld, *Phys. Rev. Lett.* 97, 218101 (2006).
30. H. C. van de Hulst, *Light Scattering by Small Particles*, Dover Publications (1981).
31. G. Popescu, Quantitative phase imaging of nanoscale cell structure and dynamics, *Methods in Cell Biology*, edited by P. J. Bhanu, Elsevier (2008), p. 87.
32. L. O. Reynolds and N. J. McCormick, *J. Opt. Soc. Am.* 70, 1206 (1980).
33. J. M. Schmitt and G. Kumar, *Appl. Opt.* 37, 2788 (1998).
34. M. Hunter, V. Backman, G. Popescu, M. Kalashnikov, C. W. Boone, A. Wax, G. Venkatesh, K. Badizadegan, G. D. Stoner, and M. S. Feld, *Phys. Rev. Lett.* 97, 138102 (2006).
35. J. D. Wilson and T. H. Foster, *Journal of Biomedical Optics* 12 (2007).
36. J. R. Mourant, J. P. Freyer, A. H. Hielscher, A. A. Eick, D. Shen, and T. M. Johnson, *Appl. Opt.* 37, 3586 (1998).
37. G. Popescu and A. Dogariu, *E. Phys. J.* 32, 73 (2005).
38. S. A. Alexandrov, T. R. Hillman, and D. D. Sampson, *Opt. Lett.* 30, 3305 (2005).
39. H. Ding, Z. Wang, L. J. Millet, M. U. Gillette, J. Liu, M. Boppart, and G. Popescu, *Opt. Lett.* submitted.
40. I. T. Jolliffe, *Principal Component Analysis*, 2nd edn., Springer (2002).
41. T. W. Loong, *British Medical Journal* 327, 716 (2003).
42. M. L. Gardel, J. H. Shin, F. C. MacKintosh, L. Mahadevan, P. Matsudaira, and D. A. Weitz, *Science* 304, 1301 (2004).
43. T. D. Pollard and G. G. Borisy, *Cell* 112, 453 (2003).
44. T. J. Mitchison and L. P. Cramer, *Cell* 84, 371 (1996).
45. T. D. Pollard, *Nature* 422, 741 (2003).
46. J. A. Theriot and T. J. Mitchison, *Nature* 352, 126 (1991).
47. F. Brochard and J. F. Lennon, *J. Physique* 36, 1035 (1975).
48. N. Gov, A. G. Zilman, and S. Safran, *Phys. Rev. Lett.* 90, 228101 (2003).
49. A. Zilker, M. Ziegler, and E. Sackmann, *Phys. Rev. A* 46, 7998 (1992).
50. A. Caspi, R. Granek, and M. Elbaum, *Phys. Rev. E* 66 (2002).

Received: 19 July 2009. Accepted: 5 November 2009.